Investigation of mixed ionic/nonionic building blocks for the dual templating of macro-mesoporous silica

Armand Roucher, Melanie Emo, François Vibert, Marie-José Stebe, Véronique Schmitt, Florian Jonas, Rénal Backov, Jean-Luc Blin

Investigation of mixed ionic/nonionic building blocks for the dual templating of macro-mesoporous silica

Armand Roucher[1,2], Mélanie Emo[2], François Vibert[2], Marie-José Stébé[2], Véronique Schmitt[1*], Florian Jonas[2], Rénal Backov[1,#], Jean-Luc Blin[2,*]

[1] CNRS, Univ. Bordeaux, CRPP, UMR5031, 115 Avenue Albert Schweitzer, 33600 Pessac, FRANCE.

[2] Institut Jean Barriol, UMR CNRS 7053 L2CM, Université de Lorraine, Faculté des sciences et technologies, BP 70239, 54506 Vandoeuvre lès Nancy cedex, FRANCE

[#] Present address: Massachusetts Institute of Technology (MIT), 77 Massachusetts Avenue, office 1-382, Department of Civil and Environmental Engineering, Cambridge, MA02139, USA. E-mail: backov@mit.edu

*Corresponding authors

Pr. Jean-Luc Blin
Université de Lorraine
UMR CNRS 7053 L2CM
Faculté des Sciences et Technologies
BP 70239
F-54506 Vandoeuvre-lès-Nancy cedex, France
Tel. +33 3 83 68 43 70
E-mail: Jean-Luc.Blin@univ-lorraine.fr

Dr. Véronique Schmitt
CRPP, UMR5031
115 Avenue Albert Schweitzer
F-33600 Pessac, FRANCE
Tel. +33 5 56 84 56 67
E-mail: schmitt@crpp-bordeaux.cnrs.fr

ABSTRACT

Traditional porous monoliths Si(HIPE) (High Internal Phase Emulsion), prepared from the Tetradecyltrimethylammonium Bromide (TTAB)/dodecane/water system, offer high specific surface area, mainly due to microporosity. Aside, mesoporous materials SBA-15, prepared from Pluronic P123, have a high specific surface area, but are obtained as powder, which limits their applications. Starting from the mixed TTAB-P123 surfactant, it is expected to tune the mesoporosity of Si(HIPE), while keeping their monolithic character.

The ternary TTAB/P123/water phase diagram was established by varying the weight ratio between these two surfactants. The micellar structure as well as the structural parameters of the liquid crystal domains were determined by SAXS (Small Angle X-ray Scattering). The effect of dodecane solubilization was also investigated and concentrated emulsions were formulated from the (P123/TTAB)/dodecane/water systems. After this soft matter dedicated study, the acquired knowledge was transferred toward the hierarchical porous silica generations, where the sol-gel process is involved.

Mixing P123 with TTAB, macro-mesoporous monolithic silica with an enhanced contribution of the specific surface area due to mesoporosity can be prepared. The variation of the TTAB/P123 weight ratio allows controlling the porosity at the mesoscale. Moreover, the macroporosity can be tuned by changing the preparation method, by mixing either the two micellar solutions or directly the two surfactants prior the emulsification process.

KEYWORDS: Emulsion; Mixed-system; Micellar structure; Monolith; Silica; Hierarchical porosity, Si(HIPE), Sol-gel; SAXS.

1. Introduction

Porous materials have found wide applications in many fields of chemistry such as catalysis, adsorption, electronics or environmental technology [1-5]. Their importance comes from their properties such as a high surface area, a high pore volume, and the presence of pores that allows the control of the diffusion. The use of adapted templates for the preparation of the materials permits the tuning of the pore sizes as well as the other properties in order to meet the requirements of any application and micro, meso, macro or hierarchical porous materials have been designed.

For example, mesostructured silica can be prepared from micelles or liquid crystals according to the cooperative templating mechanism or the liquid crystals templating pathway [6-10]. These materials present pore sizes between 2 and 50 nm according to the IUPAC nomenclature. They offer a relatively large pore size compared with zeolites (pore size below 2 nm) and this specificity allows the diffusion of larger molecules, but they are usually obtained as powder. The self-assembly mechanism is widely employed to prepare these ordered mesoporous materials [8,11,12] and numerous hydrogenated or fluorinated surfactant-based systems have been investigated as structure directing agents [6-10,13-15]. By this way, different kinds of materials called MCM (Mobil Crystalline Materials) [6,7], SBA (Santa Barbara) [16], MSU (Michigan State University) [17] have been obtained. Among these silica mesostructures, SBA-15 is the most widely studied. SBA-15 has been discovered in 1998 by Stucky et al. and it is prepared under strong acidic conditions by using micelles of Pluronic P123 [$(EO)_{20}(PO)_{70}(EO)_{20}$] as template [18]. SBA-15 is of peculiar interest since in addition to its regular hexagonal array of pores with a uniform diameter, a very high specific surface area and an important pore volume [18], the thick silica walls make the final material stable and resistant, as far as the ambient humidity remains low. The thick silica walls

characteristic is a specificity of the material and involves higher mechanical resistance [19,20].

Beside mesoporous materials, macroporous structures, i.e. with pore size higher than 50 nm have also been synthesized using multiple templates, such as latex spheres [21,22], solid lipid nanoparticles [23] emulsions [24-30] using either soft or hard templating methods. However, among the different templates, emulsion templating is a versatile method for the preparation of well-defined open porous monoliths [31]. Because the emulsion droplets are deformable, macroscopic samples are able to accommodate stress that arises during the gelation and shrinkage. Samples made using rigid spheres, by contrast, tend to break into small pieces that are seldom larger than a few hundred micrometers. In addition, emulsification conditions can be adjusted to produce droplets with different sizes which are typically in the micrometer range. In general, this technique involves the polymerization of the continuous phase and subsequent removal of the dispersed droplets by drying and heat treatment. This strategy has been used by Backov and coworkers to design the monolithic Si(HIPE) materials [27]. They are prepared under strong acidic conditions using concentrated emulsions from the tetradecyltrimethylammonium bromide (TTAB)/dodecane/water system as template and tetraethoxy-orthosilane (TEOS) as silica source. Another example is given by well controlled macroporosity conferred to silica monoliths by the use of Pickering emulsions with narrow drop size distributions [32]. Usually, the monolithic materials have typical polymerized high internal phase emulsion (poly-HIPE)-type interconnected macroporous network with polydisperse cell and window sizes within the micrometer range (1-100µm). These materials depict interconnected macroporosity with wormhole-like mesopore structure with a specific surface area around 800 m^2/g. Their applications when hybridized are wide, ranging from metallic-, enzymatic- or bacterial-based heterogeneous catalysis, photonic materials. When employed as hard templates for the generation of carbonaceous foams, the

fields of energy storage and conversion are reached with success through the generation of electro-chemical capacitors, electrodes for Li-ion batteries, enzymatic biofuel cell electrodes and so forth [33-38]. However, the main drawback of these materials is that only a weak fraction of their specific surface area is accessible to large molecules such as enzymes, the main part of the specific surface area (about 75%) is due to microporosity.

One way to increase the mesoscopic available surface of the Si(HIPE) consists in combining the emulsion templating mechanism, used for the preparation of the HIPE materials with the cooperative templating mechanism (CTM), developed for the synthesis of the mesostructured silica from surfactant-based systems, to get hierarchical macro-mesoporous silica. Emulsions have been prepared from the TTAB/dodecane /water system and the porosity at the mesoscale has been controlled by the presence of P123 micelles. However, since it is well known that non-ionic and ionic surfactants can interact to form mixed-systems with properties that cannot be found in individual surfactant [39-43], prior to the preparation of the hierarchical materials, we have investigated in detail the TTAB/P123/water system. The effect of dodecane solubilization has also been considered, since this oil is used to formulate the concentrated emulsions. This also allows shedding some light on the formation of the hierarchical porous silica.

2. Materials and methods

Tetradecyltrimethylammonium Bromide (TTAB) was supplied by Alfa Aesar. Pluronic P123, $(EO)_{20}(PO)_{70}(EO)_{20}$ and the alcoxysilane, tetraethylorthosilicate (≥ 99%, TEOS) were purchased from Sigma Aldrich. Dodecane was provided by Fisher Scientific. Deionized water was obtained using a Milli-Q water purification system.

2.1. Phase diagrams determination

Samples were prepared, by weighting the required amounts of surfactants, water and oil (if required) in sealed glass tubes. The homogenization of the samples was induced by mixing with a vortex stirrer or by mechanical milling. To favor homogenization, the samples were also centrifuged several times. The P123/TTAB/water phase diagram has been established by preparing samples over the whole range of surfactants concentrations, keeping them in a water bath at 23 °C until reaching thermodynamic equilibrium (after few days). Observations with the eyes combined with optical microscope equipped with cross polarizers (Olympus BX 50) were used to identify the different phases and to determine the phase boundaries. Small angle X-ray scattering measurements were additionally performed to establish the phase boundaries accurately, to confirm the nature of the different phases and to determine the space group of the cubic structures. Effect of dodecane solubilization has also been investigated for two P123/TTAB weight ratios, 0.14 and 1.30, which corresponds to some ratios used for the preparation of the materials. The corresponding mixed surfactants/dodecane/water phase diagrams have been determined according to the same methodology than for the P123/TTAB/water system.

2.2. Meso-macroporous materials preparation

Porous materials were synthesized in two different ways. The first synthetic route consists of mixing the micellar solution of TTAB (35 wt% with respect to water) and of P123 (5 wt% with respect to water) in different proportions so that the total weight of the prepared mixed micellar solution was always 3.2 g. By this way, the total quantity of surfactant in the micellar solution was varied from 8 to 33.5 wt%. Then, 1.0 g (0.833 cm^3) of 37 % HCl aq. and 1.0 g (1.06 cm^3) of TEOS were added into the previous solution and mixed by hand in a mortar until the pre-hydrolysis was complete. The emulsion was generated by adding drop by

drop 7 g (9.33 cm^3) of dodecane under manual stirring. The final disperse phase volume fraction is therefore equal to 0.648. The emulsion was then transferred into a Teflon autoclave for hydrothermal treatment at 100 °C for 24 h. The material was washed with ethanol under Soxhlet for 48 h and dried at room temperature for 3 days. Finally, the materials were thermally treated under atmospheric conditions as follow. A first temperature increase was applied at 2 °C/min until 180 °C with a 2 h plateau, followed by a second temperature ramp at 1 °C/min to reach 350 °C. Temperature was held for 2 h, then, a final temperature ramp at 1 °C/min was imposed to reach 650 °C with a 6 h plateau. The cooling process was uncontrolled and directed by the oven inertia. For the second synthesis, the two surfactants (TTAB and P123) were directly mixed (1.12 g total of surfactant with P123/TTAB weight ratios of 0.33, 1 and 3) and water was added until having a total weight of 3.2 g. Then, the emulsion formulation is the same as described above.

2.3. Characterization

Small angle X-Ray scattering (SAXS) data were collected on a "SAXSess mc²" instrument (Anton Paar), using line-collimation system. This instrument is attached to a ID 3003 laboratory X-Ray generator (General Electric) equipped with a sealed X-Ray tube (PANalytical, $\lambda_{Cu,\ K\alpha} = 0.1542$ nm) operating at 40 kV and 50 mA. Each sample was introduced in a "Special Glass" capillary for liquids and liquid crystals (Φ = 1.5 mm and 2.0 mm for micellar solutions and liquid crystals, respectively), or between two sheets of Kapton® for materials, then placed inside an evacuated sample chamber, and exposed to X-Ray beam. Scattering of X-Ray beam was registered by a CCD detector (Princeton Instruments, 2084 x 2084 pixels array with 24 x 24 µm² pixel size) at 309 mm distance from the sample. Using SAXSQuant software (Anton Paar), the 2D image was integrated into one-dimensional scattering intensities I(q) as a function of the magnitude of the scattering vector q

= $(4\pi/\lambda)\sin(\theta)$, where 2θ is the total scattering angle. Thanks to a translucent beamstop allowing the measurement of an attenuated primary beam at $q = 0$, all measured intensities can therefore be calibrated by normalizing the attenuated primary intensity. Data were then corrected for the background scattering from the cell and for slit-smearing effects by a desmearing procedure from SAXSQuant software, using Lake method. For micellar solutions, after treatment, obtained intensities were scaled into absolute units using water as a reference material.

Nitrogen adsorption and desorption isotherms were determined on a Micromeritics TRISTAR 3000 sorptometer at - 196 °C over a wide relative pressure range from 0.01 to 0.995. The pore diameter and the pore size distribution were determined by the BJH (Barret, Joyner, Halenda) method [44] applied to the adsorption branch of the isotherm.

Scanning electron microscopy (SEM) observations were performed with an HITACHI S4500 apparatus operating at 10 Kev. Intrusion/extrusion mercury porosimetry were measured with a Micromeritics Autopore IV 9500 porosimeter.

3. RESULTS AND DISCUSSION

3.1. The TTAB/P123/water phase diagram

The phase diagram of TTAB/P123/water at 23 °C is reported on Figure 1. It was determined only partially because, for high concentrations of total surfactant (> 70 wt%), a complex multiphasic domain appears. Micellar solutions are observed until 22 wt% of surfactants in the P123-rich region and until 35 wt% in the TTAB-rich region. This micellar domain is extended until higher contents of surfactants for mixed P123-TTAB system. For example, micellar solutions are observed until about 70 wt% of total surfactant for a P123/TTAB weight ratio of 1. As indicated in the P123/water [45] and in the TTAB/water [46] binary phase diagrams, at higher concentrations of surfactants, liquid crystals domains

appear. For the pure TTAB system, a hexagonal phase is detected from 37 to 57 wt% of surfactant (Fig. 1c). This hexagonal phase is stable until the incorporation of 10 wt% of P123. For the pure P123 system, from 22 to 37 wt%, a very stiff and isotropic phase appears, characteristic of cubic phases. SAXS experiments were done to identify its space group. According to the reflection lines detected at $1 : \sqrt{\frac{8}{3}} : \sqrt{\frac{11}{3}} : 2$, either the Fm3m or the Fd3m space groups can correspond to this cubic phase. However, due to the localization in the phase diagram, it can be attributed only to a direct micellar cubic phase, thus the Fm3m space group is retained. This is in agreement with the results reported by Gibaud et al. [47]. With the addition of TTAB, this cubic phase is progressively expanded with a tongue shape and it can incorporate more than 25 wt% of this ionic surfactant. From 37 wt% of P123 in water, an hexagonal phase is detected, as confirmed by both the texture observed by polarized-light optical microscopy (Fig. 1b) and by the SAXS pattern (Fig. 2a). It can incorporate up to 25 wt% of TTAB.

The structural parameters of the liquid crystal phases were determined from SAXS measurements. For the hexagonal phases, two compositions were chosen, one being TTAB-rich for which the ratio between the two surfactants is 0.11 (green dashed-line on Fig. 1a) and one being P123-rich for which the ratio between the two surfactants (P123/TTAB) is 9 (blue dashed-line on Fig. 1a). The corresponding diffractograms are shown in Figures 2b and 2a. For both ratios, only one hexagonal phase is observed by SAXS, suggesting the existence of a mixed entity. Assuming this hypothesis, the structural parameters of the P123-rich hexagonal phase (H_1^P) and of the TTAB-rich hexagonal phase (H_1^T) have been determined. For a given composition the d-spacing (noted d) is related to the hydrophobic radius R_H, by the following equation [48]:

$$\frac{V_B}{V_S + \alpha V_W} = \frac{\sqrt{3}\,\pi\, R_H^2}{2\, d^2}$$

where α stands for the number of molecules of water per molecule of surfactant, V_B, V_S, V_W respectively stand for the molar volumes of the hydrophobic part of the mixed surfactant, the surfactant and water (V_W = 18 cm^3/mol). V_B and V_S depend on the ratio of the two surfactants.

The cross sectional molecular area S can be deduced as:

$$S = \frac{2\,V_B}{N\,R_H}$$

N is the Avogadro number.

Results are depicted on Figures 2d and 2e. For both hexagonal phases H_1^P and H_1^T, the d-spacing increases with the addition of water. For the samples in the TTAB-rich hexagonal phase (H_1^T), the hydrophobic radius R_H and the area per polar head S are constant, equal to 1.7±0.1 nm and 0.57±0.01 nm², respectively. Considering that the TTAB alkyl chains length is around 2.0 nm, one can assume that the TTAB chains are extended in the core of the cylinders (R_H = 1.7 nm) and the dimension of the core is not modified by the presence of P123. For the samples in H_1^P region the hydrophobic radius R_H slightly decreases from 4.5 nm to 4.0 nm with the incorporation of water, while the area of the polar head S slightly increases from 1.3 to 1.5 nm². Estimating that the length of the PPO-part of the P123 is equal to 24.5 nm (1 PPO = 0.35 nm), we have thus to consider that the molecules are bent in the core of the cylinders and the hydrophobic chains adopt a meandering conformation in the H_1^P phase. For the cubic phase, the studied ratio was 2.33 (purple dashed-line on Figure 1a). The SAXS spectra are represented on Figure 2c. In this case, the relation between the cell parameter a ($a = d_{111}\sqrt{3}$) and the hydrophobic radius R_H becomes [48]:

$$\frac{V_B}{V_S + \alpha\,V_W} = \frac{16\,\pi\,R_H^3}{3\,a^3}$$

The cross-sectional area S can then be deduced from the following relation [48]:

$$S = \frac{3V_B}{N R_H}$$

On Figure 2f, the hydrophobic radius R_H of the cubic phase slightly decreases from 4.4 nm to 4.0 nm with incorporating water, while the area of the polar head *S* remains constant and equal to 0.9 nm².

Secondly, SAXS experiments were performed to investigate the micellar structure. The obtained scattering data were analyzed by the generalized indirect Fourier transformation (GIFT) [49], taking into account the inter-particles interactions. The GIFT method allows to determine the pair distance distribution function (PDDF), which corresponds to a histogram of the distances inside the particles. For the pure P123 micelles, the interactions have been calculated considering hard spheres. When the micellar solutions were composed of the Pluronic P123 and the cationic surfactant, another structure factor model was chosen. This model can be used for charged species and is called "the hypernetted-chain (HNC) closure". More details about these models and the calculations of the structure factor S(q) can be found in the literature [50]. Figures 3a-c and 3e-g represent the SAXS spectra for the pure micelles and the corresponding pair distance distribution functions (PDDFs). The spectrum of pure P123 micelles exhibits a broad peak at 0.57 nm^{-1}, characteristic of the form factor (Fig. 3a). For the P123 micelles, the PDDF exhibits a bell-like shape, characteristic of spherical micelles, with a maximum dimension of 20 nm (Fig. 3c). Additionally, the curve presents a small bump at around 5 nm, featuring the inhomogeneity of the entity (called « core-shell » type particles), as expected. The excess-electron density profile can be obtained from the deconvolution of the PDDF (Fig. 3d). It confirms the « core-shell » structure of the P123 micelles and the total radius is found at 9.3 nm. The hydrophobic radius can be defined when $\Delta\rho(r)$ changes of the sign and is thus evaluated at 3.9-4.0 nm. As the dimension of the PPO-part is about 24.5 nm, the PPO chain in the micelles is self-folded and it rather adopts a meandering conformation. This result is similar to the ones obtained for the P123-rich liquid

crystal phase. On Figure 3e, the spectrum of pure TTAB micelles shows two broad peaks at 0.7 and 1.2 nm^{-1} (grey arrows on the figure). The first one can be attributed as a correlation peak and is due to the structure factor (interparticles interaction). The second peak is characteristic of the condensation of the counterions (Br^-) around the micelles forming a shell, as described for the CTAB micelles in a previous study [51]. For TTAB micelles, the PDDF also presents a bell-like shape, whose maximum dimension is 2.1 nm, but beyond this value some oscillations appear. This behavior is typical for spherical micelles of ionic surfactants [50]. Given that the length of the TTAB molecules can be evaluated to 2.0 nm, the chains are therefore folded in the TTAB micelles.

Then, micellar solutions for different ratios of P123/TTAB were investigated by SAXS. The ratios P123/TTAB chosen were 19, 9, 3, 1 and 0.33, corresponding to the molar ratio n_{P123} / n_{TTAB} 1.1, 0.53, 0.18, 0.058 and 0.019 respectively. Looking at the mixed micellar solutions (Fig. 4a), the scattered intensity of the P123-rich micellar solutions is lower than the one of the pure P123 micelles. The spectra for the mixed TTAB-rich micellar solutions present also smaller scattering intensity than the pure TTAB micelles (Fig. 4b). This decrease of the scattering intensity features the increase of the interactions with the addition of the cationic surfactant. Jansson et al. observed the same phenomenon after adding several quantities of hexadecyltrimethylammonium chloride (CTAC) in a P123 aqueous solution at 5 wt%. [50]. Furthermore, considering the calculations of linear combinations of spectra of the pure P123 micelles and the pure TTAB micelles, the broad peak at 0.57 nm^{-1} observed for the P123 micelles remains more or less pronounced depending on the concentration of P123 for the various P123/TTAB ratios (Fig. 5b). However, looking at the experimental spectra obtained for surfactant mixtures (Fig. 5a), this peak is not visible. This means that either mixed micelles or two types of micelles with different structures than the pure ones, are formed. For the solution at a P123/TTAB ratio of 19, the SAXS spectrum presents a broad

peak as for pure P123 micelles, but it is shifted to higher q values ($q \approx 0.73$ nm^{-1}) and it is less pronounced (Fig. 5a). The obtained scattering data were analyzed by the generalized indirect Fourier transformation (GIFT). The results are presented in Figures 4c-d. Like for pure P123 micelles, the curve exhibits a bell-like shape, characteristic of spherical particles, with a maximum dimension at around 14-15 nm. Additionally, like for the P123 micelles, the PDDF presents a small bump at around 4 nm, featuring the inhomogeneity of the system. The excess-electron density profile has also been determined (Figure 4e) and confirms the « core-shell » structure of the P123-TTAB micelles and the hydrophobic radius was found at 2.5 nm. This indicates that with the addition of small quantities of TTAB, the P123-TTAB micelles have a smaller size than the pure P123 micelles, but the shape remaining the same, as observed also by Jansson et al [50]. Interestingly, the dimension of the shell remains almost constant, for this small amount of cationic surfactant. This suggests that, the TTAB chains interact with the PPO core of the P123 but the charged polar head does not modify the behavior of the PEO corona at this concentration Wyn-Jones et al observed the same behavior when adding TTAB to F127 solutions [52]. They assumed that the hydrated PEO chains in the shell are relatively « free » in the micelles and thus it is not so easy for the cationic surfactant to bind to these chains, especially at these small concentrations of TTAB. For 10% of TTAB in the mixture, the intensity of the broad peak becomes very low and for 25% of TTAB it has disappeared. According to Jansson et al [50] and Wyn-Jones et al [52] two types of complexes would be formed, due to the breaking-down of mixed P123-TTAB micelles into smaller aggregates and even monomers of P123. For 25% of TTAB, TTAB-like micelles are formed (Fig. 5a) and for higher concentrations (Fig. 4b), the shape of the scattering curves are similar to the one observed for TTAB micelles but the intensity is lower. This indicates that P123 monomers are associated with TTAB micelles. The obtained scattering data were analyzed by the generalized indirect Fourier transformation (GIFT). The results are presented

in Figures 4f-g. Like for pure TTAB micelles, the mixed micelles are spherical and their size is 1.6 and 1.8 nm for 50% and 75% of TTAB in the mixture, respectively. The sizes of these micelles are slightly smaller than that found for TTAB-micelles. The addition of TTAB involves a decrease of the micelles size as if the P123 molecules are not aggregated anymore in the micelles. These P123 molecules remain as monomer in aqueous solution in the limit of the critical micellar concentration and the other are associated with TTAB molecules (Fig. 5c).

3.2 Dodecane incorporation: the TTAB: P123/dodecane/water phase diagrams

After the study of the behavior of the mixture of the two surfactants in water, we have scrutinized the influence of dodecane toward this mixed system where two P123/TTAB weight ratios (0.14 and 1.3) have been considered (orange and pink dashed line on Figure 1a). The corresponding phase diagrams at 23 °C are shown on Figures 6a and b, respectively. For the system with the P123/TTAB weight ratio of 0.14 and below 42 wt% of surfactant, up to almost 5 wt% of oil for the highest concentrations of surfactants can be solubilized in the micelles. By contrast the hexagonal phase (from 48 to 67 wt% of total surfactant) can incorporate until 10 wt% of dodecane (Fig. 6a). A cubic phase appears after the addition of a low dodecane quantity (5 wt%) for surfactants/water ratios (R) between 1.1 and 1.8. This phase can incorporate up to 16% of dodecane. Additionally, in the oil-rich domain, concentrated oil-in-water (O/W) emulsions (CE) are prepared (from 70 wt% to 98 wt% of oil). For the system with the P123/TTAB weight ratio of 1.3 (Fig. 6b) and up to 65 wt% of surfactants, micelles can solubilize up to 2 wt% of oil. The liquid crystal domain is limited to the cubic phase from R = 1 to R = 2.3 after adding a very low amount of oil (1%). In the oil-rich domain, concentrated O/W emulsions are also obtained (from 70 to 98 wt% of oil).

The cubic phases have been characterized by SAXS for the two systems. The obtained reflection lines are $1 : \sqrt{\frac{8}{3}} : \sqrt{\frac{11}{3}} : 2$, as found for the system without oil and so identified as a direct micellar Fm3m cubic phase. The lattice parameter *a* is related to the hydrophobic radius R_H, by the following equation [48]:

$$\frac{V_B + \beta V_O}{V_S + \propto V_W + \beta V_O} = \frac{16\ \pi\ R_H^3}{3\ a^3}$$

where β and Vo stand for the number of molecules of oil per molecule of surfactant and the molar volume of the oil, respectively (Vo = 227 cm^3/mol).

Then, the cross sectional area *S* can be deduced as :

$$S = \frac{3(V_B + \beta V_o)}{N\ R_H}$$

For the direct hexagonal phase, the d-spacing is related to the hydrophobic radius R_H, by the following equation [48]:

$$\frac{V_B + \beta\ Vo}{V_s + \alpha\ V_w + \beta\ V_o} = \frac{\sqrt{3}\,\pi\,R_H^2}{2\ d^2}$$

With the system having a P123/TTAB weight ratio of 0.14, at R = 1.5, the calculated hydrophobic radius is equal to 1.9 nm for the hexagonal phase, which contains 4.5 wt% of dodecane and 3.7 nm for the cubic phase containing 15 wt% of dodecane. The corresponding area of the polar head is estimated at 0.6 nm^2 for both liquid crystal phases. The found values are in the same range than the values calculated above for the system in the rich-TTAB region without oil. With the system having a P123/TTAB weight ratio of 1.3, at R = 1.5, R_H is equal to 5.2 nm in presence of 15 wt% of dodecane, and S is evaluated at 0.8 nm^2.

Finally, highly concentrated emulsions were studied. The systems are stable for several weeks. For the systems with a P123/TTAB weight ratio of 0.14 and of 1.3, the concentrated emulsions exist for surfactants/water ratios in the range $0.09 < R < 0.47$ (Fig. 6a) and $0.08 < R < 0.28$ (Fig. 6b), respectively. SAXS experiments were done on samples

containing different amounts of oil. The spectra are shown on Figure 7. For all the studied oil concentrations, SAXS spectra present intensity proportional to q^{-4} at low q-values, characteristic of the presence of big drops. For the system with a P123/TTAB weight ratio of 0.14, at R = 0.43, at higher q-values, a well-defined peak ($q \approx 0.8$ nm^{-1}), which becomes less pronounced when increasing the concentration of oil, is present (Fig. 7b). For R = 0.11, two broad peaks ($q \approx 0.6$ nm^{-1} and 1.1 nm^{-1}) are observed (Fig. 7a). The same observations can be done for the system with a P123/TTAB weight ratio of 1.3. However, for this system, the high q-value peak is less pronounced, until becoming invisible for high concentrations of oil (Fig. 7c-d). For both systems, the position of the peak at high q values corresponds to the presence of micelles swollen by dodecane (Fig. 7e-f). The spectra feature is characteristic of systems with two phases. The diffusion proportional to q^{-4} indicates the presence of big oil drops, which are stabilized by the two types of surfactants and the peaks at higher q values are the signature of the swollen micelles [53]. The big oil drops correspond to the disperse phase while the swollen micelles in water constitute the continuous medium, which is limited to a film whose thickness decreases with the dispersed volume fraction.

The scattered intensity I(q) of these concentrated emulsions can be defined by the following equation [54]:

$$I(q) = \frac{2\pi \cdot S_V \cdot I_S(q)}{q^4} + (1 - \Phi_V) I_m(q)$$

where the first term represents the diffusion due to large particles and is approximated by Porod-Auvray's law, with S_v the specific surface and I_s is a function of the scattering length density Q profile at the water /oil interface and can be expressed as:

$$I_S(q) = (Q_{ext} - Q_{int})^2$$

where Q_{ext} and Q_{int} represent the scattering length densities of the external and internal phase of the emulsion respectively. The second term I_m can be defined as the contribution of the continuous phase.

According to the previous equations, the specific area S_V can be calculated. Then, the corresponding radius (surface-averaged radius) of oil droplets *r* can be estimated as:

$$r = \frac{3\,\Phi_V}{S_V}$$

where Φ_V is the dodecane volume fraction .

The results are given in Table 1 for 90, 95 and 98 wt% of oil. It is important to note that, the number of points in the portion of the curve with a scattering proportional to q^{-4} is limited, the error on the calculation of the radius of the big drops can thus be important. Consequently, the calculated values given in Table 1 have to be considered as an estimation only.

3.3. Silica Macro-mesoporous materials

In all cases, the porous materials have been prepared from oil-rich emulsions and the dodecane volume fraction has always been kept at 0.65. Since Si(HIPE) are obtained from pure TTAB solution (at 35 wt% with respect to the aqueous phase) [27], the TTAB-rich domain has been privileged. In a first set of experiments, micellar solutions of P123 and TTAB have been mixed prior to emulsification of the dodecane. The P123/TTAB weight ratio has been varied from 0.0075 to 1.28. The chosen proportions of P123/TTAB solutions are thus changed from 5/95 to 90/10. These values correspond to a variation of the total surfactant concentration in the P123/TTAB/water system from 33.5 to 8 wt%. The investigated compositions are marked by red circles on Figure 1a.

When considering the SAXS patterns depicted on Figure 8A, no reflection line is detected for samples prepared with a P123/TTAB ratio lower than 0.14, meaning that the materials adopt a completely random channel array. N_2 adsorption-desorption isotherms that can be qualified as intermediate between type I and IV are observed (Fig. 8B). According to Dubinin [55], these kinds of isotherms are characteristic of super-microporous materials, *i.e.* the pore size is located at the limit between the micro and mesoporous domains. This feature

was confirmed with the pore size distribution, which shows mesopore size lower than 2.0 nm, as shown in Figure 8C. Increasing the P123 content, a broad peak characteristic of a wormhole-like mesostruture, as observed for MSU, is detected at 4.0 nm (Fig. 8A). This peak gives an indication of the average pore-to-pore distance in the disordered wormhole framework, which presents a lack of long-range crystallographic order. It is shifted toward smaller q values, when the P123/TTAB ratio is raised (Fig. 8A) This vermicular mesopore arrangement is adopted by the classical Si(HIPE) [27]. The nitrogen adsorption-desorption isotherms are type IV, characteristic of mesoporous materials, according to the IUPAC classification [56]. With the increase of the P123/TTAB ratio, the pressure at which the capillary condensation occurs, is slightly shifted towards higher relative pressure. Since the pore diameter is related to the relative pressure *via* the Kelvin's equation, it can be inferred that the mesopore size increases with the P123 content. This trend is confirmed by the mesopore size distribution, whose maximum is shifted from 2.6 to 4.2 nm, when the P123/TTAB ratio varies from 0.14 to 1.28. Looking at the values reported in Table 2, it can be seen that the BJH specific surface area increases strongly with the P123 content. It varies from 281 m^2/g for P123/TTAB = 0.0075 to 918 m^2/g for P123/TTAB = 1.28. Increasing from 0.34 to 0.98 cm^3/g (Table 2) with the P123 content, the pore volume follows the same trend.

Scanning Electron Microscopy (SEM) images represented in Figure 9A show that monolithic materials are recovered. In addition, for all these materials, the structure looked quite similar while bearing a rather polydisperse distribution of macropores. For the low P123/TTAB ratio, the structure is mainly composed of open spherical shells. We can also notice that the continuous phase has not been completely mineralized conferring an additional porosity also called external path of voids or external windows. Conversely, by increasing the P123/TTAB ratios from 0.048 to 0.43, due to the chosen preparation method described in the experimental section, the total amount of surfactants decreases from 10 to 4.5 wt% and the

number of connecting windows in the walls is reduced. For the sample prepared with a P123/TTAB ratio of 0.43, the emulsion is unstable, partly due to the low quantity of surfactant. Moreover, for this ratio the TTAB molecules interact with the P123 monomers and are not available to stabilize the big drops of dodecane. This destabilization of the emulsion for the P123/TTAB weight ratio of 0.43 is characterized by the presence of large external voids between the drops fingerprints due to the coalescence phenomenon. However, the materials were synthesized at 100 °C, where condensation kinetics is very fast so that the emulsion did not have time to completely destabilize.

The macropores size distribution has been determined by mercury porosity (Fig. 9B). Whatever the investigated P123/TTAB ratio, one rather broad component centered between 9 and 15 µm is detected. It can be attributed to the macro cell windows. However, with the increase of the Pluronic content, its intensity decreases and a second component around 45 µm appears. This observation also supports the fact that the destabilization of the emulsion begins when the P123 content is raised and that the coalescence of the oil droplets occurs. The porosity features are summarized in Table 3 for a constant oil volume fraction (Φ_v = 0.65). Depending on the P123/TTAB ratio, the percentage of porosity varies from 84 to 93%, these values are higher than the one obtained for the Si(HIPE) [27]. The skeleton densities in the range of 0.23-0.50 g/cm^3 are lower than for classical Si(HIPE) (> 1g/cm^3) [27]. This densities difference can be due to the presence of micelles. We can note that the higher the P123 content, the lower the skeleton density. Moreover, in comparison with the Si(HIPE), the evolution of the parameters, characteristics of the porosity, is consistent with the increase of the BJH specific surface area due to the development of the porosity at the mesoscopic level. Additionally, the presence of the voids path also contributes to the porosity.

The macro-mesoporous materials have been synthesized from concentrated emulsions formulated from the (P123/TTAB)/dodecane/water system, considering the TTAB-rich part of

the P123/TTAB/water system. The oil droplets are thus stabilized mainly by TTAB, but we cannot exclude that a part of the P123 molecules also participate to this stabilization. As regard to the continuous medium, it is composed of the P123-TTAB mixed entities, which are swollen by the dodecane. The investigation of the micellar structure by SAXS has shown that at high TTAB content, only one type of TTAB-rich micelles is formed. So, when the TEOS is added, it interacts preferentially both with the surfactant at the surface of the oil droplets leading to the formation of the macropores, and around the TTAB-rich micelles involving the formation of the mesopores network. In both configurations, hydrolyzed TEOS moieties ensure silica clusters nucleation and growth preferentially on oil droplets and micelles, acting as defects, where the heterogeneous nucleation enthalpy is minimized when compared with the homogeneous one [27]. Due to the small size of the mixed micelles, the mesopore size is around 2.0 nm. The recovered macro-mesoporous silica present similar features than the classical Si(HIPE) in term of macroporosity, but with a BJH specific surface area of 300 m^2/g (60 m^2/g for Si(HIPE) [27]), the specific surface area due to mesopores has been enhanced. Increasing the P123/TTAB ratio, in accordance with the investigation of the L_1 micellar domain, it can be inferred that two types of micelles are in equilibrium. Indeed, big size P123-rich micelles and small size TTAB-rich micelles compose the continuous medium. As a consequence, after mineralization the obtained hierarchical silica exhibits larger mesopore diameters and the BJH specific area strongly increases to reach a value around 900 m^2/g. The development of the porosity at the mesoscale level has a drawback on the macroporosity. Indeed, as shown by SEM, with the increase of the Pluronic content, the destabilization of the emulsion occurs. However, as indicated above, thanks to the mineralization kinetics the emulsion does not have time to be completely destabilized. It should also be outlined that when P123 is used alone, we did never obtain self-standing monolith materials but powdered ones. The mechanism of formation of these hierarchical materials can be explained by a

combination of the CTM mechanism which governs the formation of the mesopore network and a templating process, in which the silica source interacts with the surfactant surrounding the oil droplets creating casts of the morphological macropores. Moreover, by changing the P123/TTAB weight ratio, one can tune the size of the mesopores.

In a second set of experiments, the total surfactant concentration in water has been fixed to 35 wt%, value used for the classical Si(HIPE). Prior to the emulsification with 65% of dodecane, the surfactants have been mixed before the preparation of the micellar solution. The surfactant concentration in the emulsion is thus 12.6 wt%. The proportion of P123 in the surfactants mixture has been varied from 0 to 75%, this corresponds to a variation of the P123/TTAB weight ratio from 0.33 to 3 (blue squares on Figure 1). Concerning the porosity at the mesoscale level the same trend than the one obtained with the preparation method described above is observed. Indeed, wormhole-like mesostucture is identified by SAXS (Fig. 10A), the broad peak is shifted towards smaller q values with the increase of the P123/TTAB ratio. The mesopore diameter increases from 3.0 to 4.3 nm when the P123/TTAB ratio is varied from 0.33 to 3.0 (Fig. 10C and table 4). The variation of the mesopore size is due to the presence of bigger entities when the P123 content is increased, as evidenced by the investigation of the micellar structure by SAXS. The identical micelles obtained through the two preparation methods show that they are at thermodynamic equilibrium as expected. The main difference concerns the macroporosity that does not result from a thermodynamic equilibrium. Indeed, as it can be seen on Figure 11, using this preparation method, smaller sizes are obtained. For example, the pore size distribution of the hierarchical silica synthesized with a P123/TTAB ratio of 0.33 presents 2 maxima at 1.8 and 6.7 µm. Depending on the preparation method, i.e. mixing the two micellar solutions or directly the two surfactants prior to the emulsification, the macropores size can thus be tuned. Increasing the P123 content the intensity of the peaks decreases and for a P123/TTAB ratio of 3, no pore is

detected in the macropores range (Figure 11B). This is also shown by the SEM images depicted on Figure 11A. This result supports the fact that increasing the Pluronic content, destabilization of the emulsion occurs. Moreover, this evolution is in good accordance with the evolution of the emulsion domain, which is progressively reduced when the P123/TTAB ratio increases (Fig. 6).

4. Conclusion

Materials exhibiting dual or hierarchical porosities have today attracted widespread interest for industrial applications and generated fascination in materials science [57,58]. Among them, monolithic Si(HIPE) are of peculiar interest, but despite a high specific surface area (800 m^2/g) only a weak fraction is accessible to large molecules, such as enzymes, since the main part is due to microporosity. To enhance the accessibility of the surface area, one way consists in increasing the mesoporosity. In this context, we have associated the high mesoporosity of SBA-15, prepared using Pluronic P123 with the monolithic aspect of Si(HIPE) to get hierarchical monoliths from the (P123/TTAB)/dodecane/water system. Prior to the emulsions formulation, the TTAB/P123/water system has been investigated. Then, the ternary TTAB/P123/water phase diagram has been studied. It shows a large domain of direct micellar phase. The micellar structure, investigated by SAXS, showed that with the incorporation of TTAB in the P123 micelles, first P123-TTAB mixed micelles with smaller sizes than the pure P123 micelles are formed, then two types of micelles coexist and finally TTAB-P123 mixed micelles are obtained. The effect of dodecane solubilization has been investigated and the concentrated emulsions were obtained and characterized. Then monolithic hierarchical silica materials have been prepared. The synthesized macro-mesoporous monoliths are highly porous (porosity around 90%) and exhibit lower bulk and skeleton densities than the conventional Si(HIPE) materials thanks to the enhanced

mesoporosity. The mesopore network adopts a wormhole-like structure. The mesopore diameter can be tuned by varying the P123/TTAB weight ratio: the higher the P123/TTAB ratio the larger the mesopores. However, a too high Pluronic content has a negative effect on the macroporosity because of the destabilization of the emulsions. It should be outlined that hierarchical porous materials are often obtained as powder [24,28,59,60] and barely as monolith [61]. The reason to get monolithic materials is that, when dealing with monolith-based heterogeneous catalysis where both surface area and mass transport are optimized, the catalyst and the catalyzed species do not have to be separated in a final step anymore. Furthermore, these materials allow an easy path toward uni-axial flux catalysis while strongly minimizing the pressure drop.

The approach described herein will open a new way to prepare hierarchical meso-macroporous silica or hybrid organic-inorganic materials and straightforward applications toward catalysis, particularly as support where molecular hindrance of big active confined entities having a size suitable with the mesopores diameter such as some enzymes (acylases , Mucor miehei lipase…) can be minimized.

Acknowledgements

The work was financed by the ANR project n°ANR-15-CE07-0023: « Intensified & Sustainable Enzymatic Acylation Processes on Innovative Macroporous/Mesoporous Materials ».

References

[1] P. Botella, A. Corma, M. Quesada, J. Mater. Chem. 22 (2012) 6394.

[2] S.Y. Park, M. Barton, P. Pendleton, Colloid Surface A 385 (2011) 256.

[3] X. Zhang, V. Thavasi, S.G. Mhaisalkar, S. Ramakrishna, Nanoscale 4 (2012) 1707.

[4] L. F. F. P. G. Braganca, M. Ojeda, J.L.G. Fierro, M.I. Pais da Silva, Appl. Catal. A-Gen. 423-424 (2012) 146.

[5] M. Arruebo WIREs Nanomed. Nanobiotechnol. 4 (2012) 16-30.

[6] C. T. Kresge, M. E. Leonowicz, W. J. Roth, J. C. Vartuli, J. S. Beck, Nature 359 (1992) 710.

[7] J. S. Beck, J. C. Vartuli, W. J. Roth, M. E. Leonowicz, C. T. Kresge, K. D. Schmitt, C. T. W. Chu, D. H. Olson, E. W. Sheppard, S. B. McCulle, J. B. Higgins J. L. Schender, J Am Chem Soc. 114 (1992) 10834.

[8] Y. Wan, D. Zhao, Chem. Rev. 107 (2007) 2821.

[9] I. Park, T.J. Pinnavaia, Microporous and Mesoporous Mater. 118 (2009) 239.

[10] K.Z. Hossain, A. Sayari, Microporous and Mesoporous Mater. 114 (2008) 387.

[11] C. T. Kresge, W. J. Roth, Chem. Soc. Rev. 42 (2013) 3663.

[12] J. L. Blin, M. Impéror-Clerc, Chem. Soc. Rev. 42 (2013) 4071.

[13] J.L. Blin, M.J. Stébé, Microporous and Mesoporous Mater. 87 (2005) 67.

[14] S.E. Rankin, B. Tan, H.J. Lehmler, K.P. Hindman, B. Knutson, Microporous and Mesoporous Mater. 73 (2004) 197.

[15] J. Esquena, C. Rodriguez, C. Solans, H. Kunieda, Microporous and Mesoporous Mater. 92 (2006) 212.

[16] D. Zhao, Q. Huo, J. Feng, B.F. Chmelka, G.D. Stucky, J. Am. Chem. Soc. 120 (1998) 6024.

[17] S.A. Bagshaw, E. Prouzet, T.J. Pinnavaia, Science 269 (1995) 1242.

[18] D. Zhao, J. Feng, Q. Huo, N. Melosh, G.H. Fredrickson, B.F. Chmelka, G.D. Stucky, Science 279 (1998) 548.

[19] A. Galarneau, M. Nader, F. Guenneau, F. Di Renzo, A. Gedeon, J. Phys. Chem. C 111 (2007) 8268.

[20] T. Benamor, L. Vidal, B. Lebeau, C. Marichal, Microporous and Mesoporous Mater. 153 (2012) 100.

[21] B.T. Holland, C.F. Blanford, A. Stein, Science 281 (1998) 538.

[22] T. Sen, G.J.T. Tiddy, J.L. Casci, M.W. Anderson, Chem. Mater. 16 (2004) 2044.

[23] R. Ravetti-Duran, J.L. Blin, M.J. Stébé, C. Castel, A. Pasc, J. Mater. Chem. 22 (2012) 21540.

[24] A. Imhof, D.J. Pine, Nature 389 (1997) 948.

[25] H. Zhang, G.C. Hardy, M.J. Rosseinsky, A.I. Copper, Adv. Mater. 15 (2003) 78.

[26] B.P. Binks, Adv. Mater. 14 (2002) 1824.

[27] F. Carn, A. Colin, M.F. Achard, H. Deleuze, E. Sellier, M. Birot, R. Backov J. Mater. Chem. 14 (2004) 1370.

[28] T. Sen, G.J.T. Tiddy, J.L. Casci, M.W. Anderson Microporous and Mesoporous Mater. 78 (2005) 255.

[29] C. Zhao, E. Danish, N.R. Cameron, R. Kataku, J. Mater. Chem. 17 (2007) 2446.

[30] S. Zhang, J. Chen, Polymer 48 (2007) 3021.

[31] G. Ceglia, L. Mahéo, P. Viot, D. Bernard, A. Chirazi, I. Ly, O. Mondain-Monval, V. Schmitt, Eur. Phys. J. E 35 (2012) 31.

[32] M. Destribats, B. Faure, M. Birot, O. Babot, V. Schmitt, R. Backov, Adv. Funct. Mater. 22 (2012) 2642.

[33] N. Brun, B. Julian-Lopez, P. Hesemann, L. Guillaume, M.F. Achard, H. Deleuze, C. Sanchez, R. Backov Chem. Mater. 20 (2008) 7117.

[34] S. Ungureanu, M. Birot, H. Deleuze, O. Babot, M.F. Achard, M.I. Popa, C. Sanchez, R. Backov Appl. Catal. A 390 (2010) 51.

[35] N. Brun, A. Babeau-Garcia, M.F. Achard, C. Sanchez, F. Durand, G. Laurent, M. Birot, H. Deleuze, R. Backov Energy Environ. Sci. 4 (2011) 2840.

[36] M. Depardieu, R. Janot, C. Sanchez, H. Deleuze, M. Morcrette, C. Gervais-Stary, R. Backov J. Mat. Chem A 2 (2014) 7694.

[37] M. Depardieu, R. Janot, C. Sanchez, A. Bentaleb, C. Gervais-Stary, M. Birot, R. Demir-Cakan, M. Morcrette, R. Backov. RSC Advances 4 (2014) 23971.

[38] V. Flexer, N. Brun, O. Courjean, R. Backov, N. Mano Energy Environ. Sci. 4 (2011) 2097.

[39] K. Ogiono, M. Abe (eds), *Mixed Surfactant Systems*, Surfactant Science Series, (1993), Vol. 46, Dekker Inc. : New York.

[40] S. Lu, J.Wu, P. Somasundaran J. Colloid Interface Sci. 367 (2012) 272.

[41] R.K. Mahajan, N. Kaur, M.S. Bakshi Colloid Surface A 276 (2006) 221.

[42] M. Almgren, V.M. Garamus, L. Nordstierna, J.L. Blin, M.J. Stébé Langmuir 26 (2010) 5355.

[43] M. Brigante, P. C. Schulz J Surfact Deterg 14 (2011) 439.

[44] E.P. Barret, L.G. Joyner, P.P. Halenda, J. Am. Chem. Soc. 73 (1951) 373.

[45] G. Wanka, H. Hoffmann, W. Ulbricht, Macromolecules 27 (1994) 4145.

[46] F. De Melo, A. Antonio, Amadeu, S. Nader, F.Y. Fujiwara, Liq. Cryst. 34 (2007) 683.

[47] S. S. Soni, G. Brotons, M. Bellour, T. Narayanan, A. Gibaud, J. Phys. Chem. B 110 (2006) 15157.

[48] M. Alibrahim, M.J. Stébé, G. Dupont, J.C. Ravey J. Chim. Phys. Phys.-Chim. Biol. 94 (1997) 1614.

[49] O. Glatter, O. Kratky, in: Small Angle X-Ray Scattering, Academic Press, (1982) 167

[50] J. Jansson, K. Schillén, M. Nilsson, O. Söderman, G. Fritz, A. Bergmann, O. Glatter, J. Phys. Chem. B 109 (2005) 7073.

[51] K. Assaker, M.J. Stébé, J.L. Blin Colloid Surface A 536 (2018) 242.

[52] Y. Li, R. Xu, S. Couderc, D.M. Bloor, J.F. Holzwarth, E. Wyn-Jones Langmuir 17 (2001) 5742.

[53] J.C.Ravey, M.J.Stébé, S.Sauvage, Colloid Surface A 91 (1194) 237.

[54] S. Rocca, M.J. Stébé, J. Phys. Chem. B 104 (2000) 10490.

[55] Dubinin, M. M. In Progress in Surface and Membrane Science 9, D.A. Cadenhead; Ed; Academic Press : New York, 1975, p. 1.

[56] K.S.W. Sing, D. H. Everett, R. A. W Haul, L. Moscou, R. A. Pierotti, J. Rouquerol, T. Siemieniewska, IUPAC, Pure and Appl. Chem. 57 (1985) 603.

[57] T. Amatani, K. Nakanishi, K. Hirao, T. Kodaira, Chem. Mater. 17 (2005) 2114.

[58] X.Y. Yang, A. Léonard, A. Lemaire, G. Tian, B.L. Su, Chem. Commun. 47 (2011) 2763.

[59] J.L. Blin, J. Grignard, K. Zimny, M.J. Stébé, Colloid Surface A 308 (2007) 7.

[60] J.L. Blin, R. Bleta, J. Ghanbaja, M.J. Stébé, Microporous and Mesoporous Mater. 94 (2006) 74.

[61] J. Nestor, A. Vílchez, C. Solans, J. Esquena, Langmuir 29 (2013) 432.

Figure caption

Figure 1: (a) Partial phase diagram of P123 / TTAB / eau at 23 °C. L_1, I_1, H_1^P and H_1^T denote the direct micellar phase, the direct micellar cubic phase and the P123-rich and TTAB-rich direct hexagonal phases respectively ; (b) Polarized-light microscopy of the hexagonal phase H_1^P; (c) Polarized-light microscopy of the hexagonal phase H_1^T. The red circles and the blue squares correspond to the compositions from which macro-mesoporous materials have been prepared. The dashed lines correspond to the P123/TTAB ratios equal to 0.11 (green), 0.13 (orange), 1.3 (pink), 2.33 (purple) and 9 (blue).

Figure 2: SAXS spectra of the liquid crystals when increasing the content of water for P123 / TTAB ratios equal to 9 (a), 0.11 (b) and 2.33 (c) at 23 °C. The grey arrows indicate the reflection lines. Evolution of the structural parameters as a function of α for the P123 / TTAB ratios equal to 9 (d) for $H_1^P$and 0.11 (e) for H_1^T and 2.33 for the cubic phase (f). α is the number of molecules of water per molecule of surfactant.

Figure 3: SAXS spectra of the pure P123 micelles (a) and the pure TTAB micelles (e) at 5 wt% of surfactant in water at 23 °C in log-log representation and in absolute units ; Corresponding experimental (dotted line) and approximated (GIFT) (solid line) SAXS spectra of the pure P123 micelles (b) and the pure TTAB micelles (f) at 23 °C ; Pair-distance distribution functions (PDDFs) for the pure P123 micelles (c) and the pure TTAB micelles (g), and excess-electron density profile of the pure P123 micelles (d)

Figure 4: (a)(b) SAXS spectra of mixed micellar solutions of P123 and TTAB at 5 wt% of surfactant for different ratios of P123 / TTAB at 23 °C. The curves are represented in log-log scale and in absolute units; (c) Experimental (dotted

line) and approximated (GIFT) (solid line) SAXS spectra of the mixed P123 / TTAB micelles at the P123/TTAB ratio 19 at 23 °C ; (d) Corresponding pair-distance distribution function (PDDF); (e) Corresponding excess-electron density profile (f) Experimental (dotted line) and approximated (GIFT) (solid line) SAXS spectra at 5 wt% of the mixed micelles at the P123/TTAB ratio equal to 0.33 (red) and 1 (black) at 23 °C ; (g) Corresponding pair-distance distribution functions (PDDFs).

Figure 5: (a) SAXS spectra of mixed micellar solutions of P123 and TTAB with a total concentration of surfactant in water equal to 5 wt% at 23 °C. The P123/TTAB ratios are indicated on the right. For clarity reasons, the spectra are shifted towards the y-axis; (b) linear combinations of pure P123 micelles and pure TTAB micelles. For clarity reasons, the spectra are shifted towards the y-axis; (c) Schematic outline of the proposed different types of micelles existing with the incorporation of TTAB to P123 micelles.

Figure 6: (a) Phase diagram of (P123/TTAB = 0.14) / water / dodecane at 23 °C ; (b) Phase diagram of (P123/TTAB = 1.30) / water / dodecane at 23 °C . For both phase diagrams, CE denotes the concentrated emulsions domain.

Figure 7: SAXS spectra of the concentrated emulsions at R = 0.11 (a) and R = 0.43 (b) for P123/TTAB ratio 0.14 and at R = 0.11 (c) and R = 0.25 (d) for P123 / TTAB ratio 1.30 in absolute units and in log-log representation; SAXS spectra of the concentrated emulsions and micelles at R = 0.11 (e) and R = 0.43 (f) for P123/TTAB ratio equal to 0.14. For clarity reasons, these spectra are shifted vertically.

Figure 8: Macro-mesoporous silica: Evolution of the SAXS patterns (A), the nitrogen adsorption-desorption isotherms (B) and the mesopore size distribution (C) as

a function of the P123/TTAB weight ratio. The total surfactant concentration varies from 2.9 to 12.1 wt%.

Figure 9: Macro-mesoporous silica: Overall appearance of the synthesized materials (A) and pore size distributions obtained through mercury porosimetry (B) as a function of the P123/TTAB weight ratio. The total surfactant concentration varies from 2.9 to 12.1 wt%.

Figure 10: Macro-mesoporous silica prepared from a 19.2 wt% total surfactant concentration: Evolution of the SAXS patterns (A), the nitrogen adsorption-desorption isotherms (B) and the mesopore size distribution (C) as a function of the P123/TTAB weight ratio.

Figure 11: Macro-mesoporous silica prepared from a 19.2 wt% total surfactant concentration: Overall appearance of the synthesized materials (A) and pore size distributions obtained through mercury porosimetry (B) as a function of the P123/TTAB weight ratio.

Table 1: Specific area (S_V) and radii of oil droplets (r) estimated from SAXS measurements

P123/TTAB weight ratio	R	wt% oil	S_v (10^3 cm^{-1})	r (μm)
0.14	0.43	95	50	0.6
		90	52	0.5
0.14	0.11	98	22	1.4
		95	22	1.3
		90	11	2.6
1.30	0.25	95	93	0.3
		90	127	0.2
1.30	0.11	98	14	2.1
		95	18	1.6
		90	28	1.0

Table 2: Variation of the BET surface area, the total pore volume, the BJH surface area and the mesopore diameter as a function of the P123/TTAB weight ratio.

P123/TTAB weight ratio	BET surface area ($m^2.g^{-1}$)	Total pore volume ($cm^3.g^{-1}$)	BJH surface area ($m^2.g^{-1}$)	Average pore diameter (nm)
0.0075	644	0.34	281	< 2.0
0.016	791	0.44	377	< 2.0
0.048	796	0.40	310	< 2.0
0.14	979	0.91	918	2.6
0.43	786	0.77	808	3.3
1.28	826	0.98	918	4.2

Table 3: Variation of the porosity, the intrusion volume and the skeletal density as a function of the P123/TTAB weight ratio with a constant oil volumefraction ($\Phi_v = 0.65$).

P123/TTAB weight ratio	Porosity (%)	Intrusion volume ($cm^3.g^{-1}$)	Skeletal density ($g.cm^{-3}$)
0.048	93	27.1	0.50
0.14	93	24.6	0.58
0.43	84	22.2	0.23

Table 4: Variation of the porosity features as a function of the P123/TTAB weight ratio for porous materials prepared with 1.12 g of total surfactant.

P123/TTAB weight ratio	Porosity (%)	Intrusion volume ($cm^3.g^{-1}$)	BET surface area ($m^2.g^{-1}$)	Total pore volume ($cm^3.g^{-1}$)	BJH surface area ($m^2.g^{-1}$)	Average pore diameter (nm)
0.33	91	10.4	939	1.70	473	3.2
1.00	75	9.1	793	1.95	642	3.0
3.00	61	1.5	602	1.28	673	4.

Figure 1

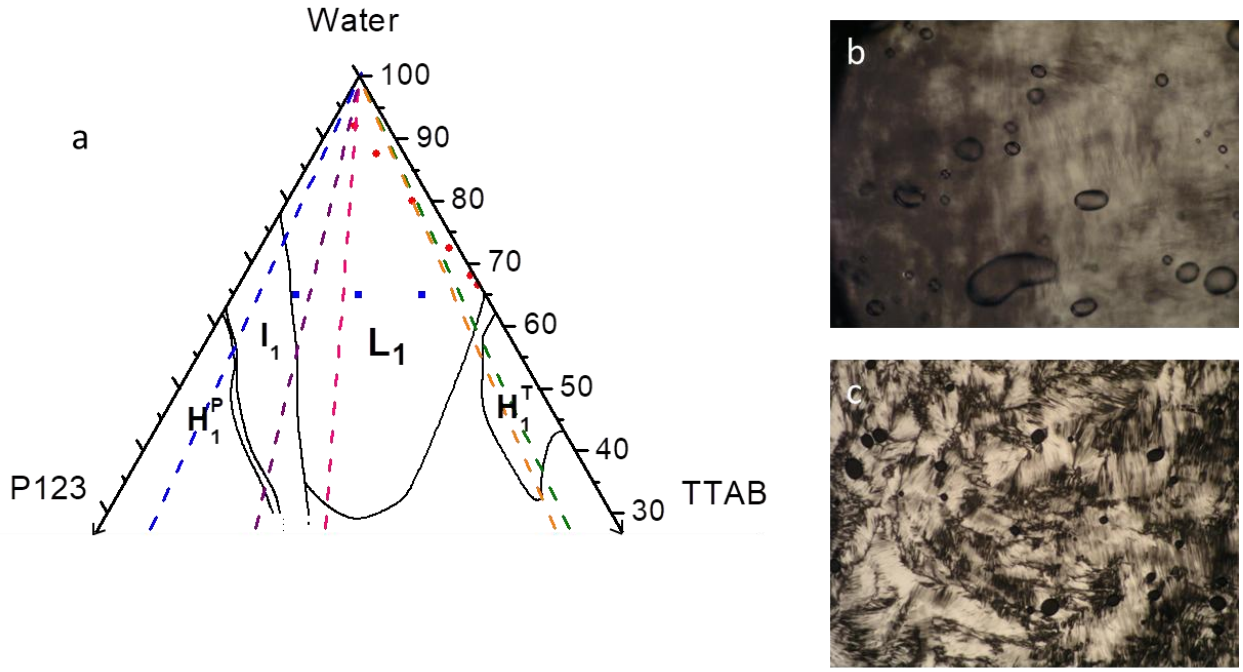

Figure 2

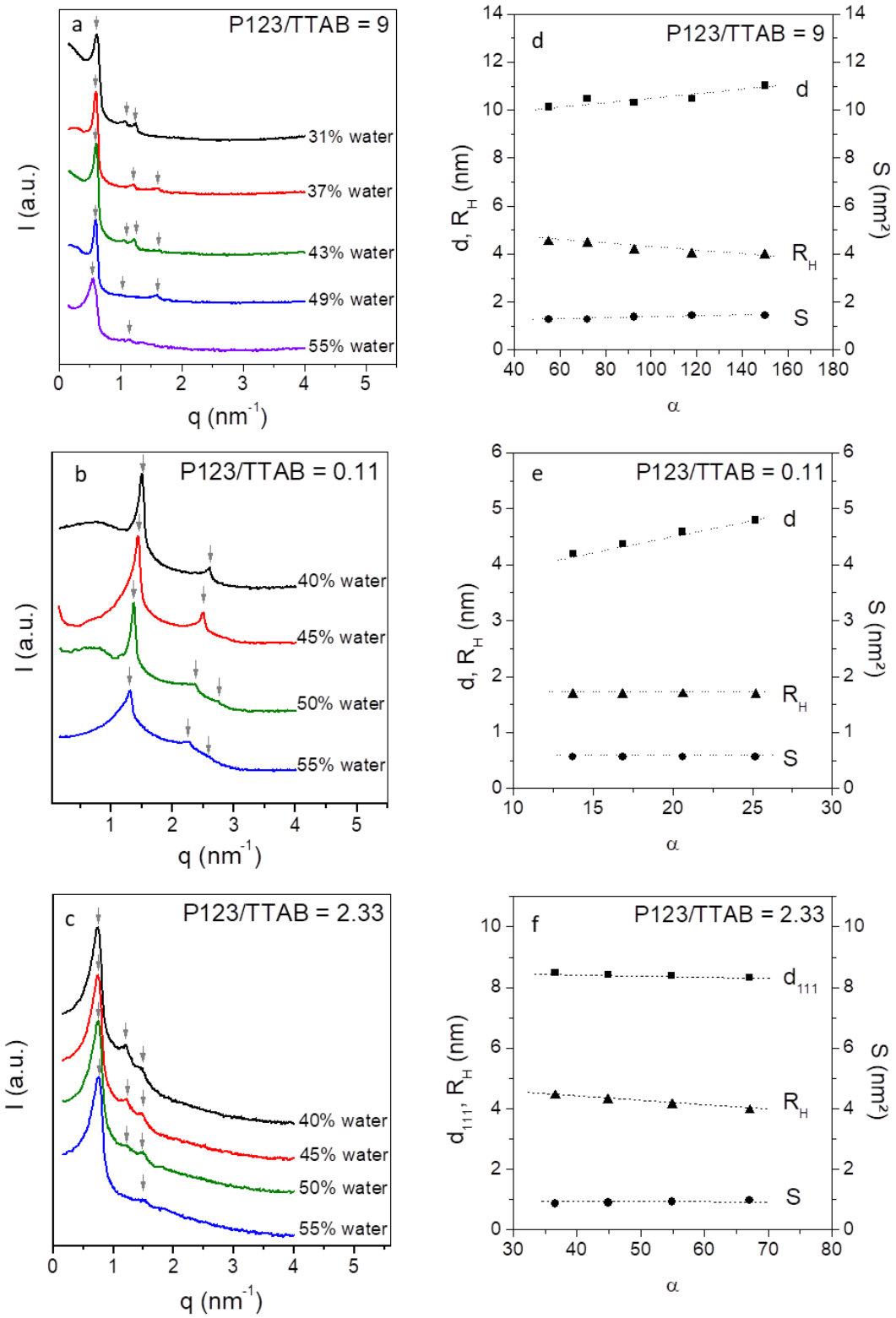
a
P123/TTAB = 9
31% water
37% water
43% water
49% water
55% water
I (a.u.)
q (nm-1)
b
P123/TTAB = 0.11
40% water
45% water
50% water
55% water
I (a.u.)
q (nm-1)
c
P123/TTAB = 2.33
40% water
45% water
50% water
55% water
I (a.u.)
q (nm-1)
d
P123/TTAB = 9
d
RH
S
d, RH (nm)
S (nm2)
α
e
P123/TTAB = 0.11
d
RH
S
d, RH (nm)
S (nm2)
α
f
P123/TTAB = 2.33
d111
RH
S
d111, RH (nm)
S (nm2)
α

Figure 3

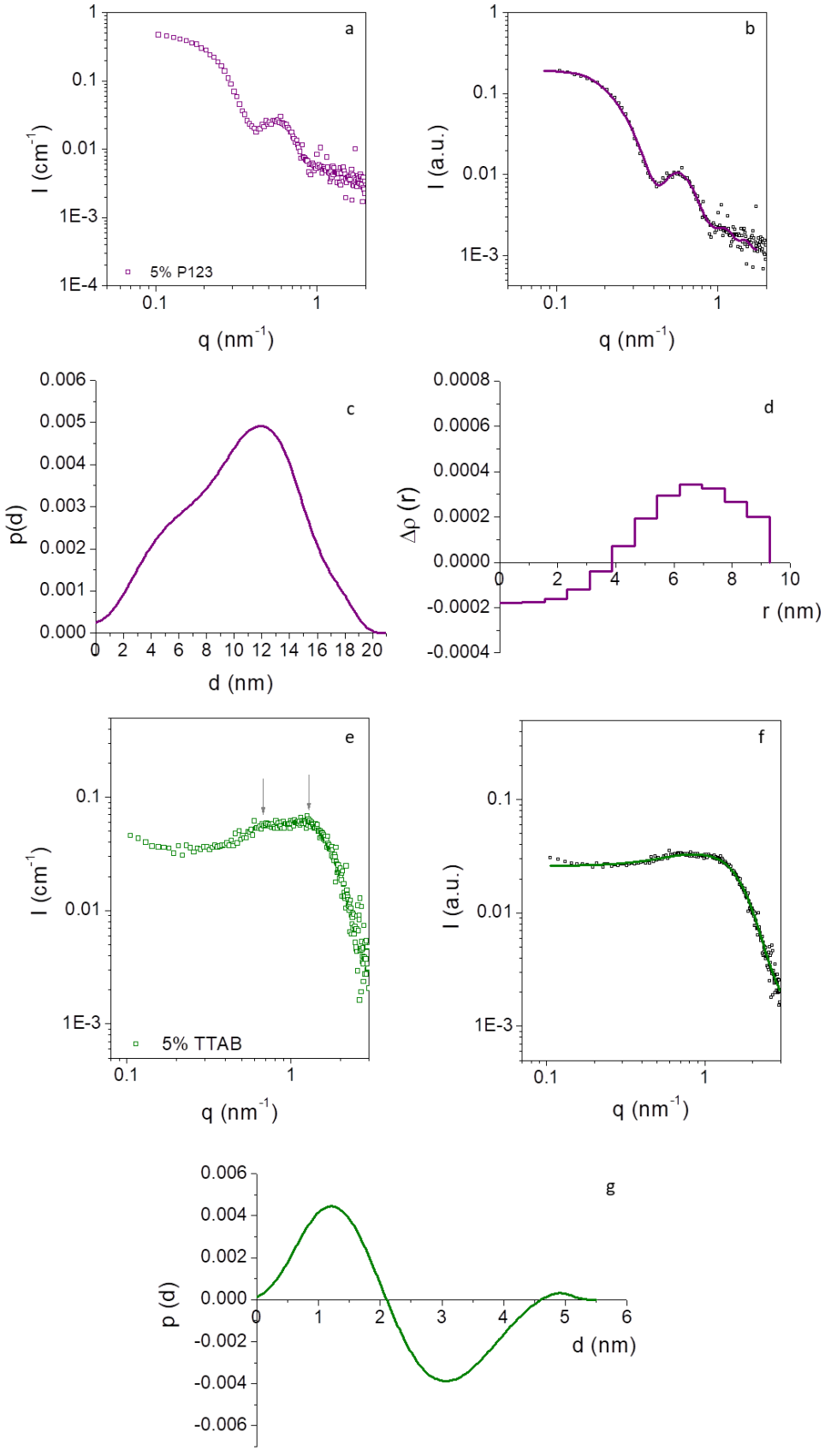
a
I (cm^{-1})
q (nm^{-1})
5% P123
b
I (a.u.)
q (nm^{-1})
c
p(d)
d (nm)
d
Δρ (r)
r (nm)
e
I (cm^{-1})
q (nm^{-1})
5% TTAB
f
I (a.u.)
q (nm^{-1})
g
p (d)
d (nm)

Figure 4

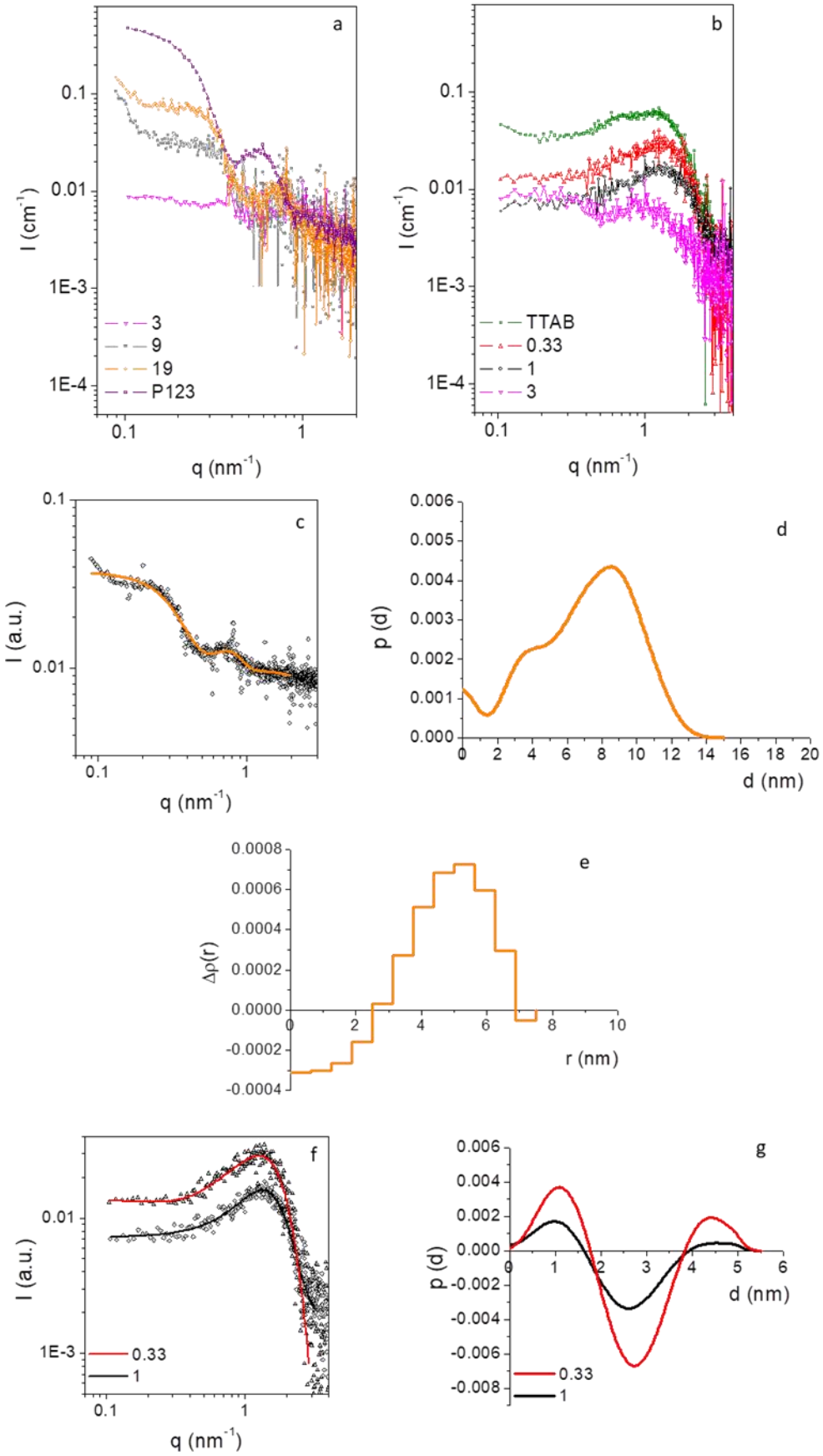
a
I (cm^{-1})
q (nm^{-1})
3
9
19
P123
b
TTAB
0.33
1
3
c
I (a.u.)
d
p (d)
d (nm)
e
Δρ(r)
r (nm)
f
0.33
1
g

Figure 5

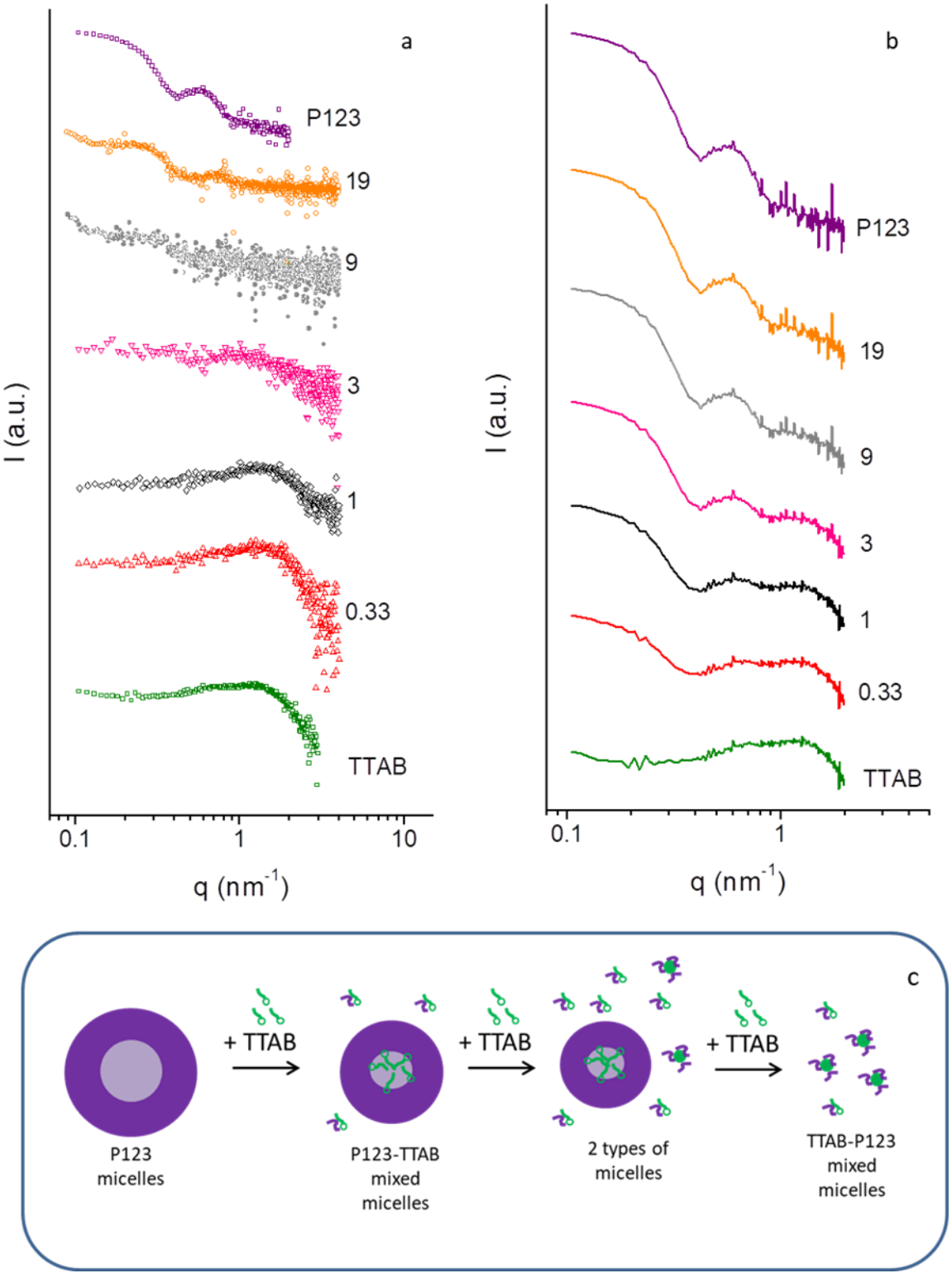
a
P123
19
9
3
1
0.33
TTAB
I (a.u.)
0.1
1
10
q (nm-1)
b
P123
19
9
3
1
0.33
TTAB
I (a.u.)
0.1
1
q (nm-1)
c
+ TTAB
+ TTAB
+ TTAB
P123 micelles
P123-TTAB mixed micelles
2 types of micelles
TTAB-P123 mixed micelles

Figure 6

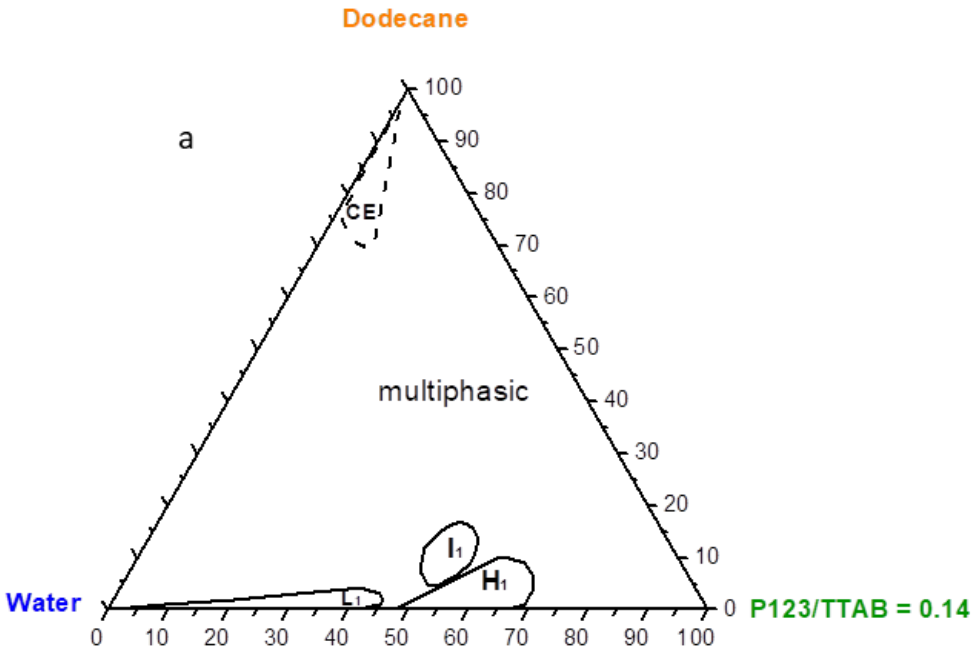
Dodecane
a
CE
multiphasic
I1
H1
L1
Water
P123/TTAB = 0.14
100
90
80
70
60
50
40
30
20
10
0
0 10 20 30 40 50 60 70 80 90 100

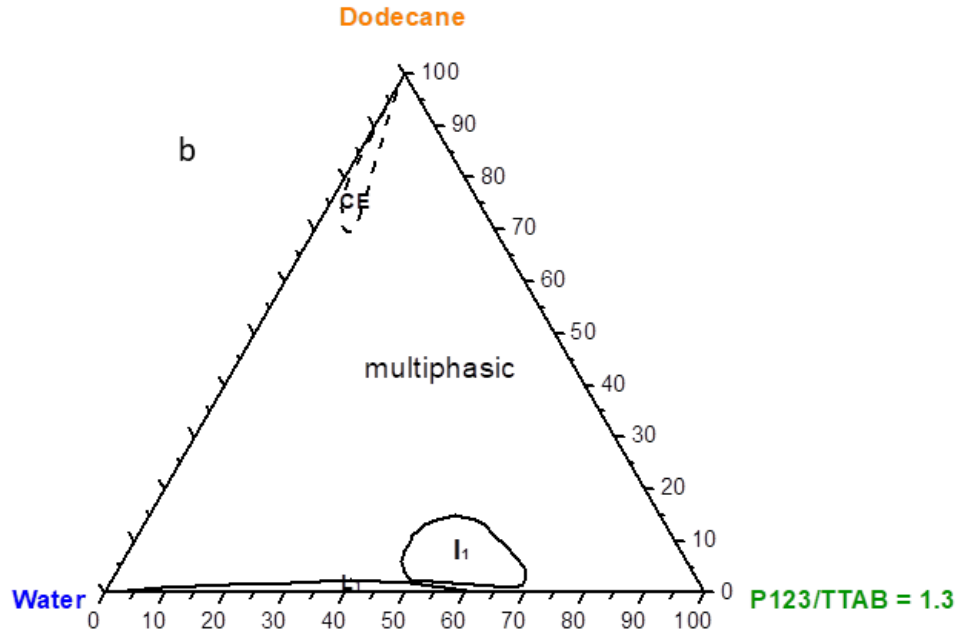
Dodecane
b
CE
multiphasic
I1
L1
Water
P123/TTAB = 1.3
100
90
80
70
60
50
40
30
20
10
0
0 10 20 30 40 50 60 70 80 90 100

Figure 7

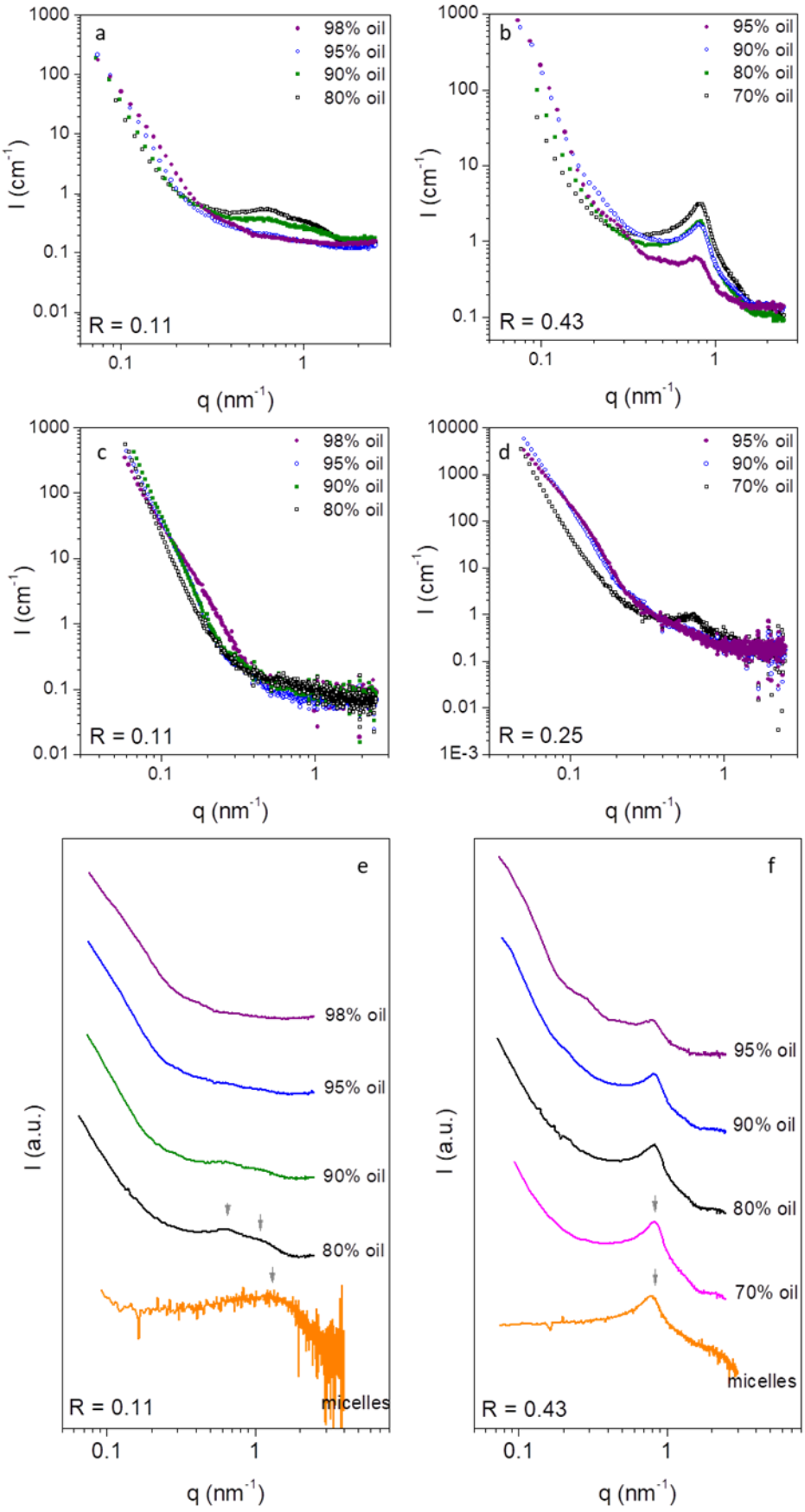
a
98% oil
95% oil
90% oil
80% oil
R = 0.11
I (cm-1)
q (nm-1)
b
95% oil
90% oil
80% oil
70% oil
R = 0.43
c
R = 0.11
d
R = 0.25
e
98% oil
95% oil
90% oil
80% oil
micelles
R = 0.11
I (a.u.)
f
95% oil
90% oil
80% oil
70% oil
micelles
R = 0.43

Figure 8

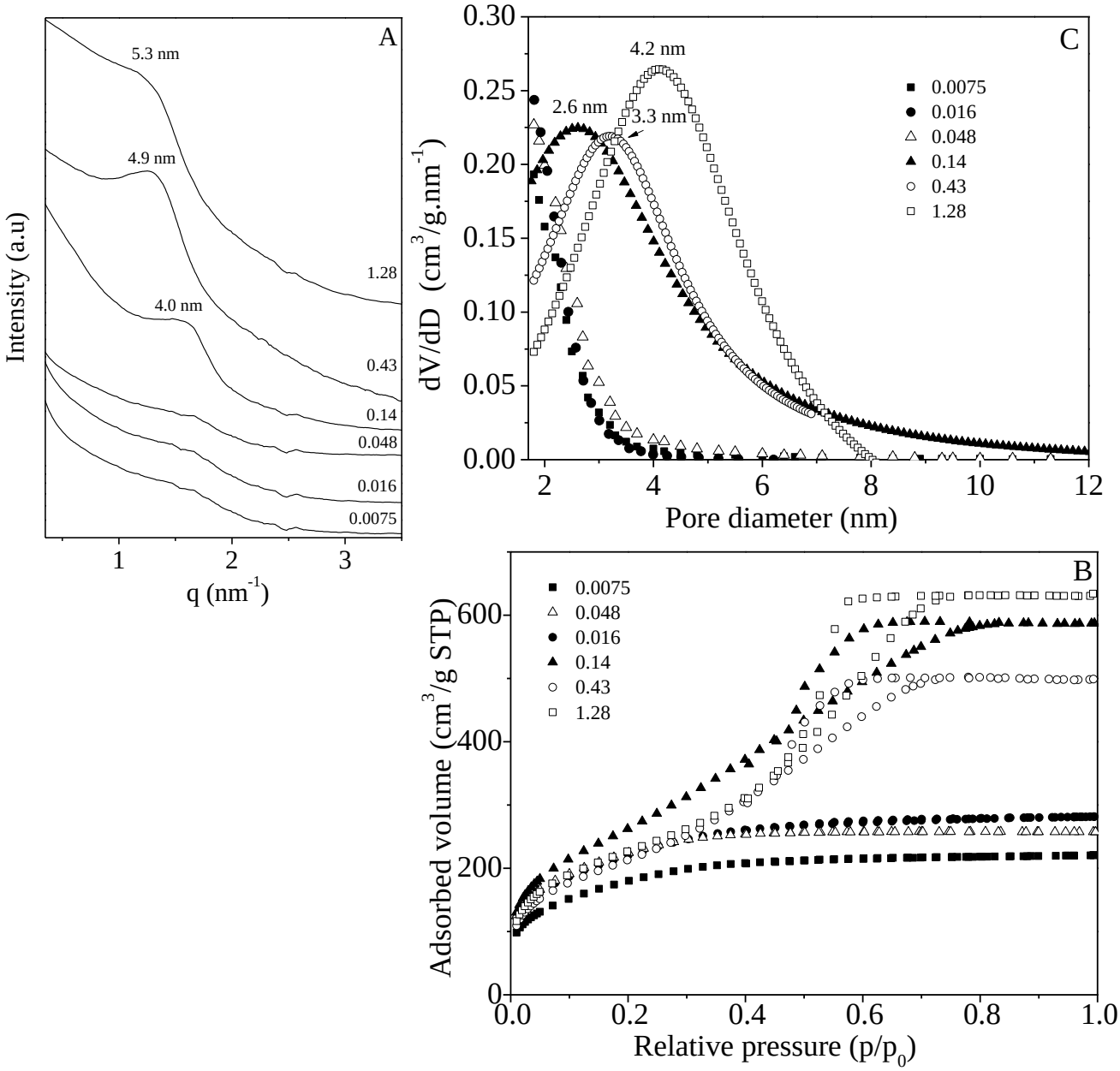
A
5.3 nm
4.9 nm
4.0 nm
1.28
0.43
0.14
0.048
0.016
0.0075
Intensity (a.u)
q (nm-1)
C
4.2 nm
2.6 nm
3.3 nm
0.0075
0.016
0.048
0.14
0.43
1.28
dV/dD (cm3/g.nm-1)
Pore diameter (nm)
B
0.0075
0.048
0.016
0.14
0.43
1.28
Adsorbed volume (cm3/g STP)
Relative pressure (p/p0)

Figure 9

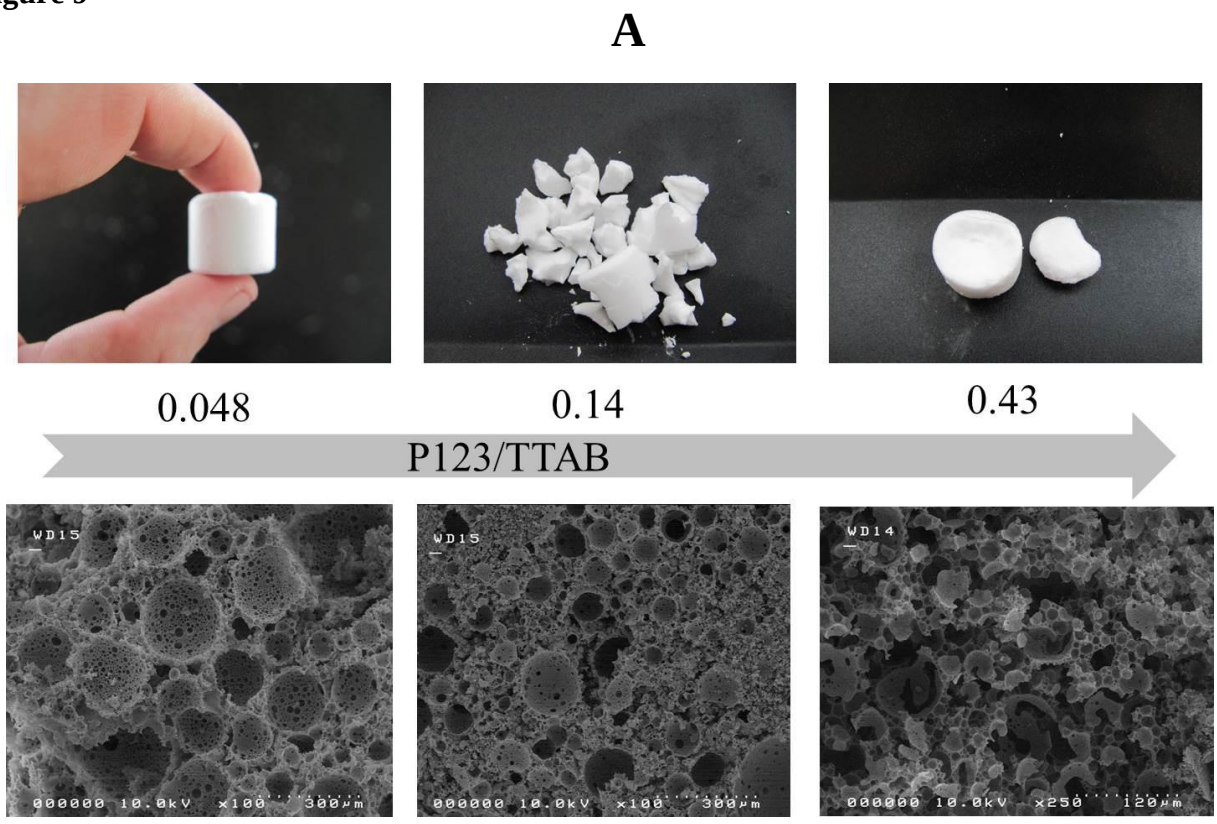
A
0.048
0.14
0.43
P123/TTAB
WD15
WD15
WD14
B
13 µm
9.5 µm
44 µm
10.4 µm
1.6 µm
0.048
0.14
0.43
Log Differential Intrusion (mL/g)
Pore Diameter (µm)
0
10
20
30
40
0.1
1
10
100

Figure 10

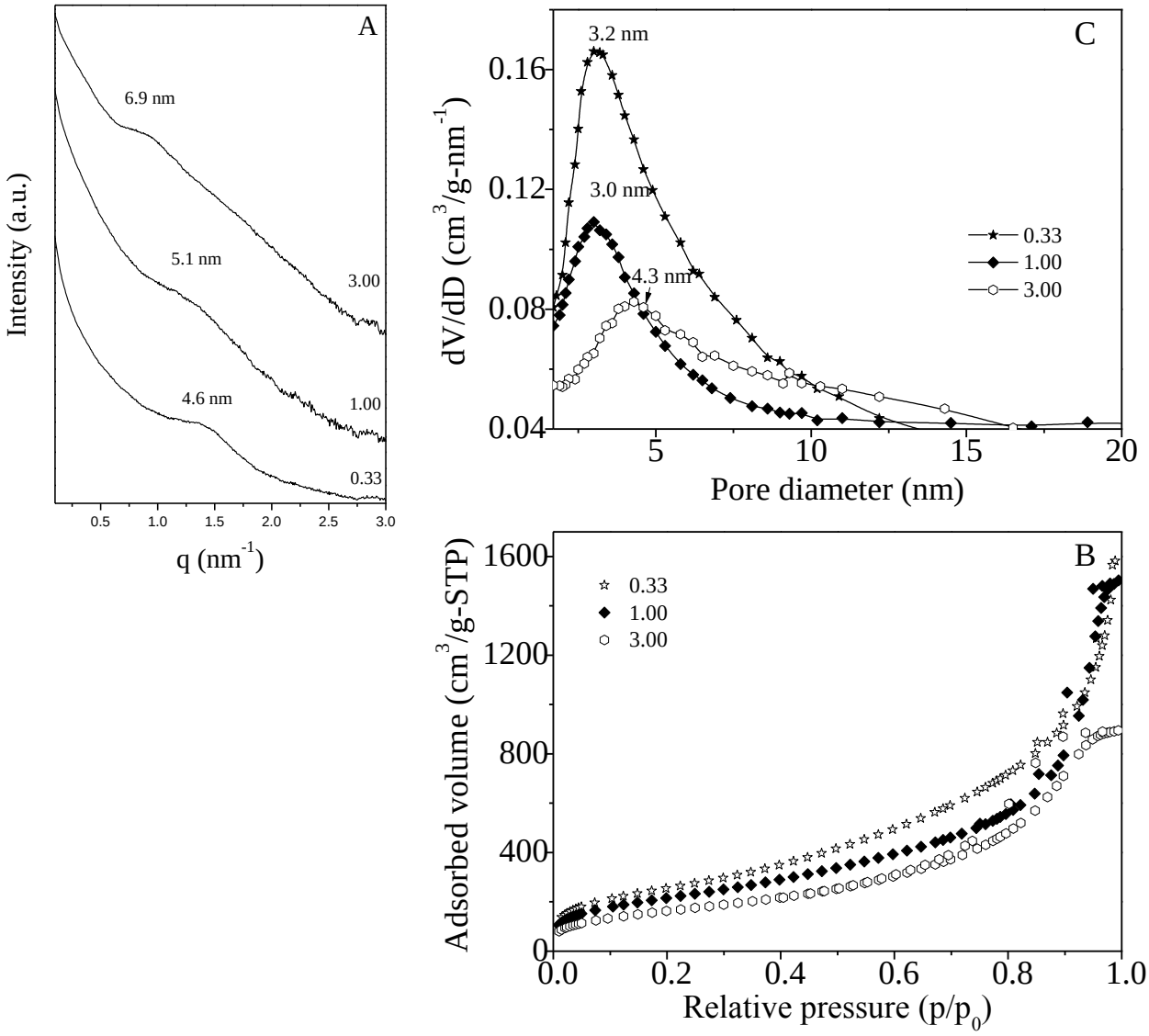
A
6.9 nm
5.1 nm
4.6 nm
3.00
1.00
0.33
Intensity (a.u.)
q (nm-1)
C
3.2 nm
3.0 nm
4.3 nm
0.33
1.00
3.00
dV/dD (cm3/g-nm-1)
Pore diameter (nm)
B
0.33
1.00
3.00
Adsorbed volume (cm3/g-STP)
Relative pressure (p/p0)

Figure 11

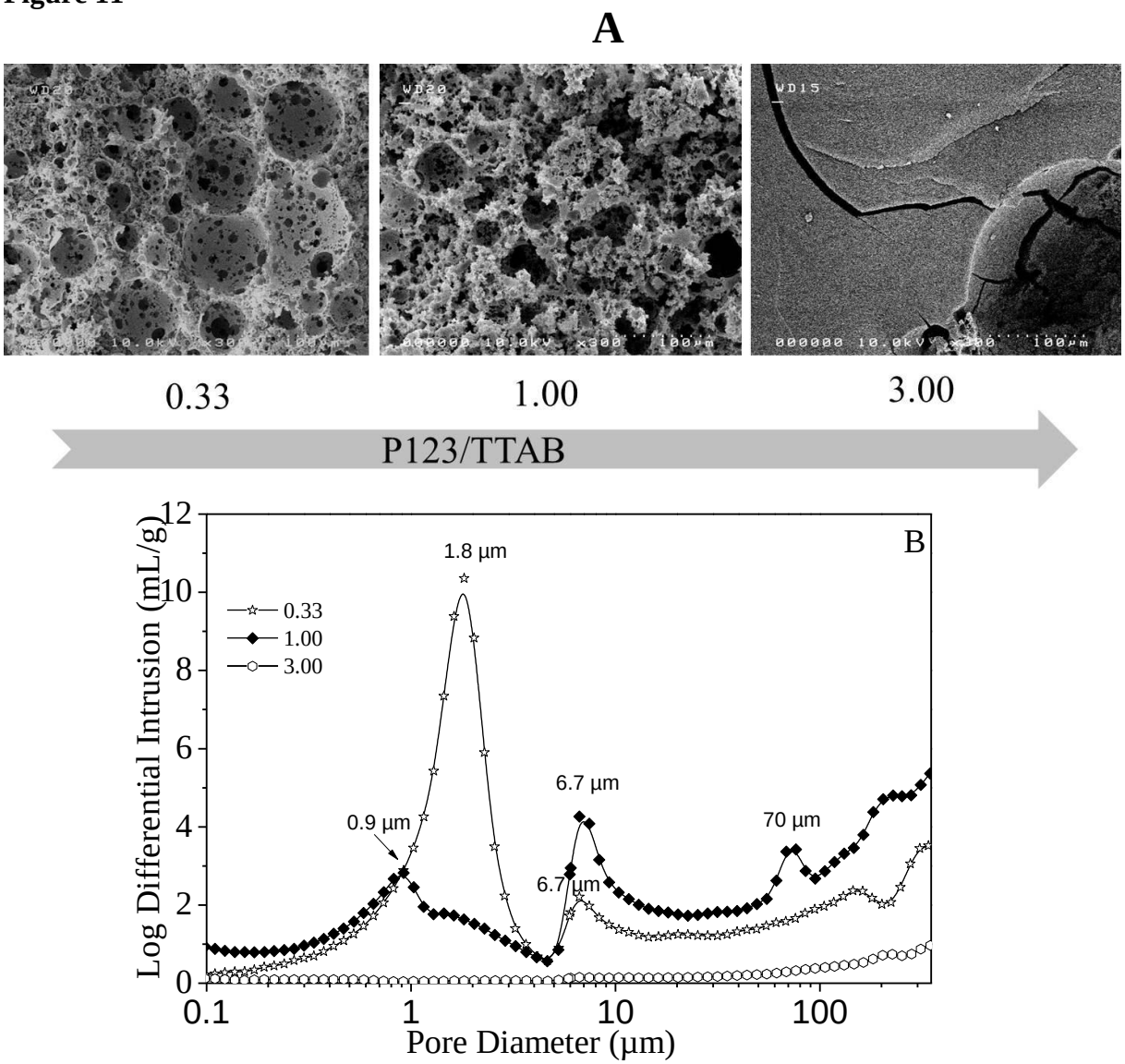
A
0.33
1.00
3.00
P123/TTAB
B
1.8 µm
0.9 µm
6.7 µm
6.7 µm
70 µm
0.33
1.00
3.00
Log Differential Intrusion (mL/g)
Pore Diameter (µm)
0
2
4
6
8
10
12
0.1
1
10
100